Solvothermal Synthesis of LiFePO 4 Hierarchically Dumbbell-Like Microstructures by Nanoplate Self-Assembly and Their Application as a Cathode Material in Lithium-Ion Batteries

ARTICLE *in* THE JOURNAL OF PHYSICAL CHEMISTRY C · FEBRUARY 2009

Impact Factor: 4.77 · DOI: 10.1021/jp808080t

4 AUTHORS, INCLUDING:

Xing-Long Wu
Northeast Normal University
62 PUBLICATIONS **3,168** CITATIONS
SEE PROFILE

Minhua Cao
Beijing Institute of Technology
129 PUBLICATIONS **4,037** CITATIONS
SEE PROFILE

Yu-Guo Guo
Chinese Academy of Sciences
170 PUBLICATIONS **10,870** CITATIONS
SEE PROFILE

Solvothermal Synthesis of $LiFePO_4$ Hierarchically Dumbbell-Like Microstructures by Nanoplate Self-Assembly and Their Application as a Cathode Material in Lithium-Ion Batteries

Hui Yang,[†] Xing-Long Wu,[§,#] Min-Hua Cao,*[,†,‡] and Yu-Guo Guo*[,§]

Department of Chemistry, Northeast Normal University, Changchun, 130024, People's Republic of China, Department of Chemistry, Beijing Institute of Technology, Beijing, 100081, People's Republic of China, and Beijing National Laboratory for Molecular Sciences, Institute of Chemistry, Chinese Academy of Sciences, Beijing 100190, People's Republic of China

Received: September 11, 2008; Revised Manuscript Received: December 16, 2008

In this work, $LiFePO_4$ with hierarchical microstructures self-assembled by nanoplates has been successfully synthesized by using poly(vinyl pyrrolidone) (PVP) as the surfactant in a benzyl alcohol system. The resulting dumbbell-like $LiFePO_4$ microstructures are hierarchically constructed with two-dimensional nanoplates with ~300 nm length and ~50 nm thicknesses, while these tiny plates are attached side by side in an ordered fashion. Both benzyl alcohol and LiI acting as reducing agents promote the formation of $LiFePO_4$, and the presence of PVP plays an important role in the construction of the hierarchically self-assembled microstructures. A reasonable formation mechanism is proposed on the basis of the result of time-dependent experiments. In addition, the cell performance of the synthesized $LiFePO_4$ is better than that of the commercial $LiFePO_4$, which makes it a promising cathode material for advanced electrochemical devices such as lithium-ion batteries and supercapacitors.

1. Introduction

Since the pioneering work of Padhi et al.,[1] lithium iron phosphate ($LiFePO_4$) has been particularly attractive with respect to its application as a positive electrode material in rechargeable lithium batteries, owing to its particular features such as high theoretical capacity (170 mA h g^{-1}), low cost, nontoxicity, and high safety. As we know, however, a main obstacle of $LiFePO_4$ is its poor electronic conductivity, which is the most unfavorable issue for the rate capability of batteries. Many attempts[2−10] have been made to overcome this limitation by coating an electronically conductive phase (typically carbon, metals, or polymers, etc.), minimizing the $LiFePO_4$ particle size, or doping with foreign atoms. In addition, some researches recently have focused on the electrochemical kinetics and mechanism studies of the lithium intercalation process for $LiFePO_4$ electrodes,[11−14] which means that the investigation of $LiFePO_4$ cathode materials is facing a deeper and more extensive development.

In recent years, however, there has been little innovation on the synthesis routes for $LiFePO_4$. The most common and traditional method to prepare $LiFePO_4$ is still the solid-state reaction synthesis.[9,15] This approach, nevertheless, suffers from the problems of complicated producing processes including grinding, ball milling, and subsequent heat treatment generally at 400−700 °C under Ar/H_2 atmosphere until the crystalline $LiFePO_4$ formed, which inevitably induces high energy consumption and large particle sizes of the product. Besides this method, the sol−gel synthesis and hydrothermal synthesis routes are also widely used. Although the sol−gel method is capable of producing gel precursors, in which multiple reactants are homogeneously mixed at the molecular level, resulting in a good morphological or particle size control, it still demands a subsequent heating treatment to obtain the crystalline $LiFePO_4$.[7,8] Furthermore, the hydrothermal method has also been reported for synthesizing crystalline $LiFePO_4$ at a low temperature, but additional reducing agents and inert gas atmosphere are always employed for prohibiting the oxidation of Fe^{2+} to Fe^{3+} due to its high reactivity in aqueous solution.[16−18] Therefore, it is still a challenge for our researchers to seek for a simple and economically efficient route at relatively low reaction temperature for the synthesis of nanoscale $LiFePO_4$ with well-defined shape and size.

Now the organization of nanoscale building blocks (nanoparticles,[19] nanorods,[20] nanoribbons,[21] and nanoplates[22,23]) into hierarchical architectures via self-assembly is becoming an intensive and hot research topic because of their improved physical and chemical properties for potential applications in optics, electronics, medicine, and energy/chemical conversions and their important roles in the systematic research of structure−property relationships. Up to now, there are few reports on the synthesis of $LiFePO_4$ hierarchical architectures with well-defined morphologies, and the reported literatures mainly involve tabular particles,[16] irregular nanoparticles,[24,25] and porous nanostructures.[4,26] Recently Dominko et al.[26] reported that $LiFePO_4$ particles with hierarchically organized pores can operate at current rates up to 50 °C while still preserving a high tap density of ca. 1.9 g cm^{-3}. Thus, it is significant to explore a reasonable synthetic method for the construction of $LiFePO_4$ hierarchical structures. Up to now, morphosynthesis of crystalline $LiFePO_4$ has scarcely been reported, mainly due to its multielement nature.

Benzyl alcohol, as one kind of high-boiling solvent, has been extensively reported for solvothermal synthesis of nanostructures in the past few years,[27−29] which has advantages such as one-

* To whom correspondence should be addressed. E-mail: caomh043@nenu.edu.cn (M.-H.C.); ygguo@iccas.ac.cn (Y.-G.G.).
[†] Northeast Normal University.
[‡] Beijing Institute of Technology.
[§] Chinese Academy of Sciences.
[#] Also at the Graduate School of the CAS, Beijing 100064, China.

10.1021/jp808080t CCC: $40.75
Published on Web 02/04/2009

step synthesis, environmental friendliness, easy operation, and good repetition. On one hand, the reactivity of different precursors in this solvent becomes slow and matches each other, which facilitates the formation of the desired multimetal oxides instead of a mixture of the individual binary oxides,[30] hence having a better control over the purity and crystallinity of final products. On the other hand, a proper surfactant in solvothermal systems could also tune the particle size and morphology owing to the adsorption of surfactant molecules onto particle surfaces during particle growth. Motivated by these advantages, we believed that the benzyl alcohol solvent would overcome the drawbacks that the aqueous solution has. Up to now, some nanostructures of relatively simple compounds, such as metal oxides, perovskites, and hybrid materials, have been solvothermally synthesized using benzyl alcohol as solvent.[29,31] To the best of our knowledge, there have been no any reports on the synthesis of multicomponent materials such as $LiFePO_4$ via the benzyl alcohol system.

In this work, we reported a facile synthesis route at low temperature for $LiFePO_4$ microstructures with dumbbell-like shape, which are self-assembled by nanoplates with ~300 nm length. $FeCl_3 \cdot 6H_2O$, H_3PO_4, and LiI were used as precursors, and poly(vinyl pyrrolidone) (PVP) was used as a soft template in benzyl alcohol. The obtained $LiFePO_4$ hierarchical microstructures show an excellent cycling stability without capacity fading up to 70 cycles when they were used as a cathode material in lithium-ion batteries

2. Experimental Section

2.1. Materials. All chemicals used were purchased without further purification. $FeCl_3 \cdot 6H_2O$ was purchased from Tianjin Yaohua Chemical Plant; LiI was from Shanghai China Lithium Industrial Co., Ltd.; PVP (K30) was from Sinopharm Chemical Reagent Co., Ltd.; benzyl alcohol was from Tianjin Fuchen Chemical Reagents Company; H_3PO_4 (85 wt % solution) was from Beijing Chemical Reagents Company.

2.2. Synthesis. The $LiFePO_4$ samples with dumbbell-like microstructures were prepared by a simple solvothermal process in the presence of PVP. In a typical synthesis, appropriate quantities of $FeCl_3 \cdot 6H_2O$, H_3PO_4 (85 wt % solution), LiI, and PVP with molar ratio of 1:1.5:10:7 were added into 60 mL of benzyl alcohol. After vigorous magnetic stirring at room temperature for 0.5 h, a wine-colored transparent solution was formed. Then this solution was transferred into an 80 mL Teflon-lined stainless steel autoclave, which was heated at 150 °C for 2 days. After being cooled to room temperature, the product was centrifuged, washed several times with absolute alcohol and distilled water, and finally dried in air for 6 h. To study the influence factors on the composition, size, and shape of the final product, the experimental parameters, such as the Li precursor and the solvent, have been varied during the synthesis. Before the measurement of electrochemical properties, the $LiFePO_4$ sample were annealed at 600 °C for 5 h (heating rate of 2 °C/min) under a mixed atmosphere of N_2 (90%) and H_2 (10%).

2.3. Electrochemical Measurements. Electrochemical measurements were performed using two-electrode Swagelok-type cells assembled in an argon-filled glovebox. For preparing working electrodes, a mixture of $LiFePO_4$ nanostructures, acetylene black, and poly(vinyl difluoride) (PVDF) at a weight ratio of 70:20:10 was pasted on an Al foil. A glass fiber (GF/D) from Whatman was used as separator. Lithium foil was used as counter electrodes. The electrolyte consisted of a solution of 1 M $LiPF_6$ in ethylene carbonate (EC)/dimethyl carbonate (DMC)/diethyl carbonate (DEC) (1:1:1, in wt %) obtained from Ferro Corporation. Galvanostatic cycling tests of the assembled cells were carried out on an Arbin BT2000 system in the voltage range of 4.2−2.2 V (vs Li^+/Li).

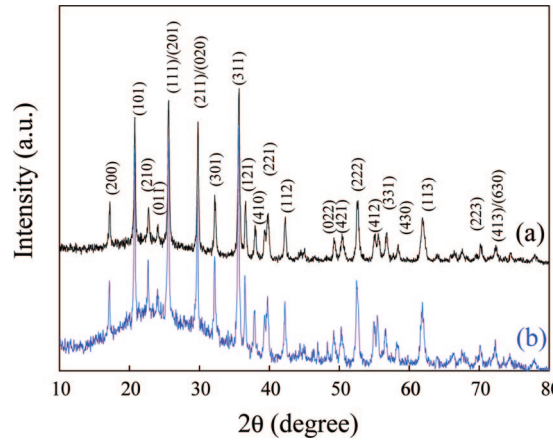

Figure 1. XRD patterns of the as-synthesized $LiFePO_4$ microstructures (a) before calcination and (b) after calcination.

2.4. Characterization. The resulting samples were characterized by X-ray powder diffraction (XRD) (Rigaku D-max-rA XRD with Cu Kα radiation). The morphology and dimension of samples were observed by field emission scanning electron microscopy (FE-SEM, JEOL 7500B) and transmission electron microscopy (TEM, H-800). The microstructure of samples was determined using high-resolution transmission electron microscopy (HRTEM) on a JEM-2010 apparatus with an acceleration voltage of 200 kV. The Fourier transform infrared spectroscopy (FT-IR) pattern was recorded on a Perkin-Elmer model 580B spectrometer from 400 to 2000 cm^{-1}. X-ray photoelectron spectroscopy (XPS, ESCALAB 250) was used to confirm the oxidation state of iron.

3. Results and Discussion

3.1. Structural Analysis and Morphology Characterization. XRD pattern of the sample prepared with PVP as the template is shown in Figure 1a. All of the diffraction peaks can be well indexed to pure $LiFePO_4$ with an orthorhombic olivine structure (JCPDS card no. 81-1173). No impurities such as Li_3PO_4 and others, which often appear in the $LiFePO_4$ product synthesized by traditional routes,[32] are observed. All diffraction peaks are strong and narrow, indicating the high crystallinity of the $LiFePO_4$ sample. XPS was used to analyze the chemical state of the atoms in the sample. The wide XPS spectrum in Supporting Information Figure S1 shows that the binding energy of Li 1s, P 2p, and O 1s are determined to be 55.8, 113.1, and 531.2 eV, respectively, with the reference binding energy at 284.6 eV for the C 1s peak. Figure 2 presents the XPS spectrum of Fe element on the surface of the sample. The binding energy positions at 712.3 and 726.2 eV are ascribed to Fe $2p_{3/2}$ and Fe $2p_{1/2}$, respectively, which perfectly match with previously reported spectra of $LiFePO_4$[33] and are characteristic of Fe^{2+} cation. Thus, the XPS analysis further confirms the purity for $LiFePO_4$ sample.

Figure 3a shows a typical low-magnification FE-SEM image of the $LiFePO_4$ sample. It can be clearly seen that the sample is mainly composed of dumbbell-like microstructures with length ranging from 1.5 to 2 μm. Parts b and c in Figure 3 display an individual $LiFePO_4$ dumbbell-like microstructure at a higher magnification, showing that the $LiFePO_4$ dumbbell-like microstructures are hierarchically constructed with two-dimensional nanoplates with ~300 nm length and ~50 nm thicknesses, while

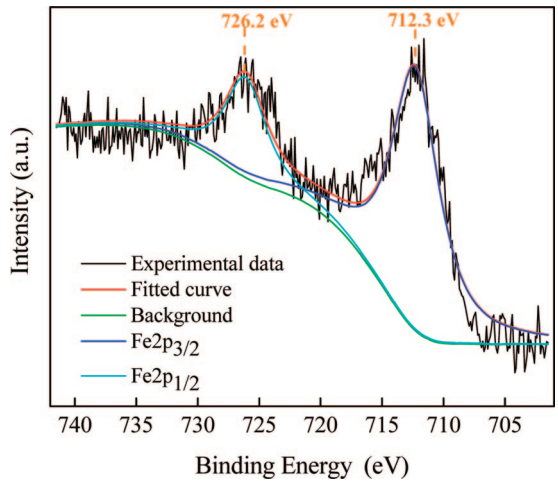

Figure 2. Fe 2p XPS spectra of the $LiFePO_4$ sample.

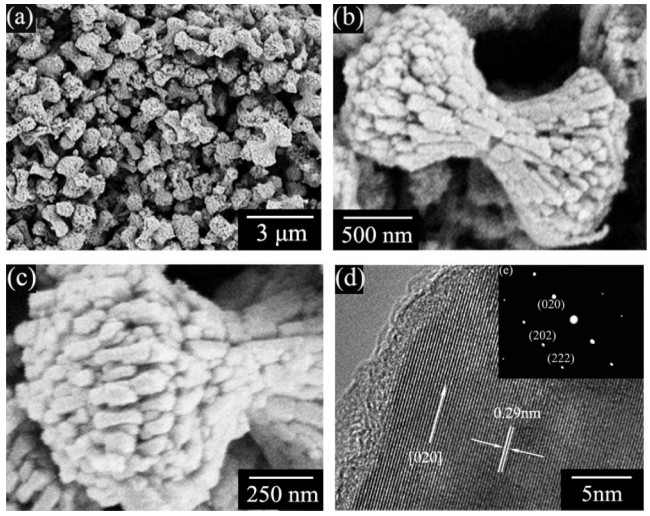

Figure 3. (a−c) Typical SEM images: (a) low-magnification and (b) an individual dumbbell-like $LiFePO_4$ microstructure from the obverse side and (c) lateral side. (d) HRTEM image of the tip of an individual dumbbell shape. (e) SAED pattern.

these tiny plates are attached side by side in an ordered fashion. Further insight into the morphology and microstructure of the $LiFePO_4$ dumbbell-like microstructures was gained using TEM and HRTEM. A typical TEM image shown in Supporting Information Figure S2 further affirms that the as-obtained sample consists of large-scale well-dispersed dumbbell-like microstructures. It is worth mentioning that these microstructures are sufficiently stable that they cannot be destroyed into fragments or dispersed nanoplates even after ultrasonic treatment. An HRTEM image (Figure 3d) taken on an individual nanoplate displays clear crystal lattices with *d*-spacing of 0.29 nm, corresponding to (020) planes of orthorhombic phase $LiFePO_4$. In addition, it can also be seen from the HRTEM image that an amorphous layer with a thickness of 2−3 nm covered the surface of $LiFePO_4$. Detailed researches about this are carried out in a later section. The selected area electron diffraction (SAED) pattern shown in Figure 3e exhibits a regular and clear rectangular diffraction spot array, which indicates that the nanoplate is single-crystalline and can be indexed as the $LiFePO_4$ orthorhombic phase.

It was found by a series of experiments that the currently used synthesis strategy provides a powerful means to tailor the composition, purity, and assembly of $LiFePO_4$ microstructures in dependence of reaction parameters such as lithium precursor, solvent, and addition of PVP. First, we discuss the effect of lithium precursor and solvent on the composition and purity of the final product. As we know, benzyl alcohol is a reduced solvent, which can partly reduce transition-metal ions. This fact has been confirmed by ref 30. However, in our experiment, a phenomenon is worth nothing that the color of the solution turned from the initial yellow (the color of Fe^{3+}) to wine-colored after the mixture of LiI benzyl alcohol solution and $FeCl_3$ benzyl alcohol solution. This color change may imply the reduction of Fe^{3+} into Fe^{2+} by I^-. This can be explained by the theoretical electrode potentials of Fe^{3+}/Fe^{2+} and I_2/I^- as follows:

$$I_2 + 2e^- \rightleftharpoons 2I^- \qquad \phi^\theta = 0.535\ \text{V}$$

$$Fe^{3+} + e^- \rightleftharpoons 2Fe^{2+} \qquad \phi^\theta = 0.770\ \text{V}$$

$$Fe^{3+} + 2I^- \rightleftharpoons Fe^{2+} + I_2 \qquad E^\theta = \phi^\theta_{Fe^{3+}/Fe^{2+}} - \phi^\theta_{I_2/I^-} = 0.235\ \text{V} > 0$$

The total electrode potential of the reaction is positive, which means the reaction is spontaneous. So it brings a question, that is, which acts as main reducing agent, LiI or benzyl alcohol? To solve this question, we performed two compared experiments by simply changing the synthesis conditions. One experiment was carried out under the same synthetic conditions but using water instead of benzyl alcohol as the solvent. The XRD pattern of resulting sample is shown in Supporting Information Figure S3a, which demonstrates that all of the diffraction peaks are indexed to pure $Fe_4(PO_4)_3(OH)_3$ (JCPDS card no. 80-0759). It means that in the absence of benzyl alcohol Fe^{2+} could be oxidized to Fe^{3+} by O_2 possibly from the water, even with the excess of LiI. The fact indicates that LiI fails to reduce Fe^{3+} species in the aqueous solution, whereas in the benzyl alcohol system it works due to the existence of a reductive environment offered by the solvent, which ensures the sufficient exertion of LiI reduction. The other experiment was conducted with other constant conditions except for replacing LiI by LiCl as Li precursor. The XRD pattern (Supporting Information Figure S3b) shows that the sample is a mixture of Li_3PO_4 (JCPDS card no. 84-0003) and $FeFe_2(PO_4)_2(OH)_2$ (JCPDS card no. 85-1728). The mixed valence states of Fe ions further provide a proof that the benzyl alcohol can only partly reduces Fe^{3+}, which is in agreement with that reported in literature.[28] Therefore, LiI used by us serves not only as the lithium precursor but also a reducing agent. On the basis of the above analyses, it can be found that both LiI and benzyl alcohol play important roles in the formation of pure $LiFePO_4$.

To highlight the influence of PVP on the assembly behavior of $LiFePO_4$, we carried out a series of compared experiments, where we only change the amount of PVP used while other reaction parameters are the same. Supporting Information Figure S4 displays SEM investigations of the $LiFePO_4$ samples obtained with different concentrations of PVP. As shown in Supporting Information Figure S4a, it is found that without PVP, irregular and nonuniform plates with a large size are formed. When 0.021 M PVP was used, three-dimensional (3D) hierarchical microstructures self-assembled by nanoplates can be detected, although the dominant products remain ill-defined and underdeveloping structures (Supporting Information Figure S4b). When the concentration of PVP increases to 0.029 M, namely, the optimum synthesized condition, a number of well-defined dumbbell-like microstructures self-assembled by nanoplates are observed as shown in Supporting Information Figure S4c. Further increase in the concentration of PVP (0.037 M) leads to the formation of dumbbell-like microstructures with larger

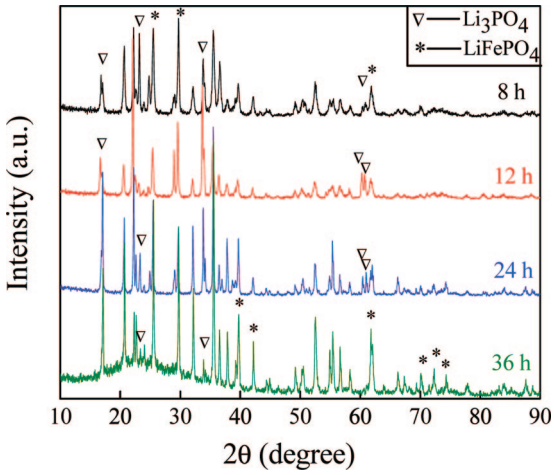

Figure 4. XRD patterns of the samples obtained at different reaction times: (black) 8, (red) 12, (blue) 24, and (green) 36 h.

length of up to 2−3 μm (Supporting Information Figure S4d). And some dumbbell-like microstructures fracture into a single sector. These observations clearly show that the presence of PVP is beneficial to construct the hierarchically self-assembled microstructures, and adjusting the amount of PVP is crucial to control both morphology and size of the $LiFePO_4$ microstructures. In fact, we tried many different surfactants, for instance, cetyltrimethyl ammonium bromide (CTAB), poly(ethylene glycol) (PEG), and Triton X-100. However, they all did not show a good oriented growth function for $LiFePO_4$ nanocrystals. The TEM images obtained with different surfactants (Supporting Information Figure S5) indicated that all of the products are irregular and nonuniform plates with a large size. So it can be seen that PVP plays a vital role in the morphology assembly. In addition, if $FeSO_4$ was used as iron precursor instead of $FeCl_3$, the hierarchically self-assembled microstructures cannot be obtained, although it has no effect on the composition of the final sample. This is why we choose $FeCl_3$ and not $FeSO_4$ as iron precursor.

3.2. Formation Mechanism. To gain insight into the formation process of the $LiFePO_4$ product, time-dependent experiments were carefully conducted. First, the prepared samples at different times were investigated by XRD. As shown in Figure 4, the XRD pattern of the product obtained at 8 h indicates that the peaks can be indexed as a mixture of $LiFePO_4$ phase and Li_3PO_4 phase (JCPDS card no. 84-0003), and the strong diffraction peaks partially belong to Li_3PO_4 phase, demonstrating the formation of Li_3PO_4 phase at the initial stage. With increasing the reaction time to 12, 24, and 36 h, the relative intensities of the diffraction peaks for Li_3PO_4 become gradually weaker, whereas the peaks of the $LiFePO_4$ phase turn to be very narrow and strong, indicating that the crystallinity is much improved. With the Li_3PO_4 phase vanished, the single $LiFePO_4$ phase is obtained until increasing the reaction time to 48 h (Figure 1a). It is obvious that there is a "phase transformation" in the formation process of pure $LiFePO_4$.

The products at different reaction stages were also inspected by TEM to reveal the growth process of $LiFePO_4$ hierarchical microstructures. Taking the high crystallinity of Li_3PO_4 phase in the initial reaction stage into account, we mainly investigate the morphological variation in the latter part of the growth stage (Figure 5). The TEM image of the sample obtained at 24 h is shown in Figure 5a, from which the rectangular structures with a large size are dominant in the sample and individual dumbbell-like microstructures are occasionally observed. The rectangular

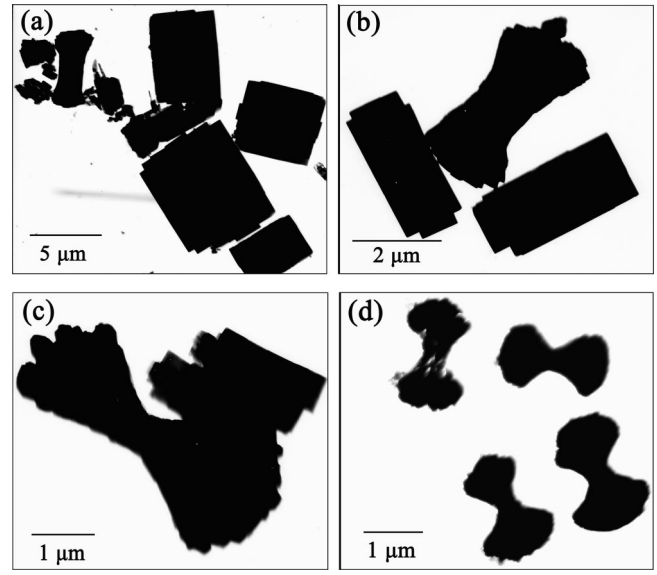

Figure 5. TEM images of the samples obtained at different reaction times: (a) 24, (b) 36, (c) 40, and (d) 48 h.

structures in fact are assembled by much smaller nanoplates, which can be confirmed by careful examination for the jagged edge and the fragmentary nanoplates around them. When the reaction time was prolonged to 36 h, the rectangular structures and dumbbell-shaped products coexist in the sample, both with uniform sizes (Figure 5b). It is worth mentioning that the size of the rectangular structures, with a length of 3−3.5 μm, is far smaller than the one for 24 h. Further prolonged to 40 h, the rectangular structures become smaller with a length of 2 μm, as shown in Figure 5c. When the reaction time was prolonged to 48 h, well-defined dumbbell-like microstructures are observed in Figure 5d, and both ends of the dumbbell-like microstructures, namely, the fanlike sectors, get gradually wider than before. There are two morphologies coexisting at the crystal formation stages, namely, the rectangular structures and the dumbbell-like microstructures. They are both assembled by nanoplates with careful examination, but their nature is not the same. From the XRD results at different reaction times (Figure 4), it is observed that the product is a mixture of Li_3PO_4 and $LiFePO_4$ when the reaction time is less than 48 h. Only when the reaction time is increased to 48 h is pure $LiFePO_4$ single phase obtained. So, it can be considered that the nature of the nanoplates is different at different reaction stages. It is a mixture of Li_3PO_4 and $LiFePO_4$ before 48 h and a pure $LiFePO_4$ phase after 48 h.

On the basis of the TEM investigations, accompanied with crystal structure and chemical composition analyses, we propose a mechanism for the formation of $LiFePO_4$ hierarchically dumbbell-like microstructures. A main evolving process is schematically illustrated in Figure 6, involving the following five steps. (1) Nucleation and growth: in the present solvothermal process, during the mixing of the reactants, massive precipitation of Li_3PO_4 nuclei formed quickly, followed by the growth of the nuclei into rectangle-shaped nanocrystals. (2) Aggregation: driven by the minimization of the total energy of the system and the interaction between PVP and crystal surface, the small primary nanoplates begin to aggregate together. Because of the instability of structures in steps 1 and 2, it cannot be inspected by TEM. FT-IR spectroscopy clearly proves the presence of PVP in our sample and the interaction between PVP and $LiFePO_4$ crystal surfaces, as shown in Figure S6 (Supporting Information). Apart from the PO_4^{3-} vibrations (900−1150 and 400−650 cm^{-1}),[34,35] the weak and narrow bands at 1629 and

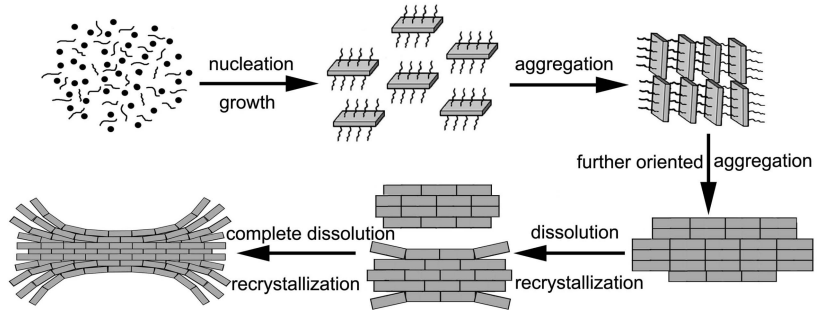

Figure 6. Schematic illustration for the formation of hierarchically dumbbell-like $LiFePO_4$ microstructures.

1653 cm^{-1} are observed, which are attributed to the stretching vibration mode of the PVP carbonyl (Supporting Information Figure S6a). From this, it can be demonstrated that the as-prepared $LiFePO_4$ sample contains a small quantity of PVP. In our case, compared to the C═O adsorption position of pure PVP at 1679 cm^{-1} (Supporting Information Figure S6b), the shift of the PVP carbonyl position is essentially assigned to the interaction of the C═O (PVP) with the $LiFePO_4$ crystal surfaces. The result is consistent with those earlier studies,[36,37] where it has been addressed that the PVP can protect the nanoparticles via the carbonyl group. In addition, this result also confirms that the amorphous shell around the $LiFePO_4$ crystal lattice seen in the HRTEM image may be due to the adsorption of PVP. (3) Further oriented aggregation: with reaction time longer, the Li_3PO_4 nanoplates further aggregate to form a pseudocubic 3D structure to reduce the surface energy (Figure 5a). (4) Dissolution and recrystallization: with the temperature and pressure increasing steadily, the solubility of Li_3PO_4 increases in the solvent. Thereby, because of the large solubility and metastability of Li_3PO_4 compared with $LiFePO_4$, this metastable intermediate phase began to decompose and recrystallized to form $LiFePO_4$ nuclei. To reduce the surface energy, the initially formed $LiFePO_4$ nanoplates began to assemble in edge-to-edge and layer-by-layer growth style,[38] just because of the PVP interaction. With a longer reaction time, however, instead of further piling up to form a cube, the previously formed structures consisting of nanoplates preferred to tilt at both ends, resulting in the formation of notched structures for further development. This specific growth fashion should be due to lattice tension or surface interaction in the edge areas.[39] (5) Complete dissolution and recrystallization: when the reaction time was close to 48 h, the Li_3PO_4 phase was almost completely dissolved. More newly formed $LiFePO_4$ nanoplates would be continually assembled onto the notched structures, resulting in thickening of the edges of structures and a stagnating growth in the middle section. Finally, the dumbbell-like structures were formed. Therefore, the formation of $LiFePO_4$ is based on a dissolution−recrystallization process, along with the phase transformation from one material to another material. Here, solubility plays an important role in determining the growth of the nanocrystals.[40] This is very similar to the previous reports for the formation of Zn_2SnO_4,[41] α-Fe_2O_3,[42] $LiCoO_2$,[43] and $NaLnF_4$.[44] In summary, it is believed that this special morphology assembly depends on many factors, for example, the intrinsic character of $LiFePO_4$, the surface interaction, the lattice tension, and PVP effect.

3.3. Electrochemical Properties. Before the electrochemical measurements, the $LiFePO_4$ sample was heated to 600 °C in inert atmosphere. As we know, the surfactant itself remains more or less in the final product for the liquid-phase synthesis, even after being rinsed many times with distilled water. Taking it into account, we annealed the pristine $LiFePO_4$ sample. On one hand, annealing can remove the left surfactant; on the other hand, it can transform the surfactant into carbon to enhance the electronic conductivity. Hence, PVP in the system can be considered not only as the surfactant to tailor the morphology, but also as a carbon source. The CHN elemental analysis indicates that the amount of carbon in the calcined $LiFePO_4$ sample is about 1 wt %, implying only a small quantity of PVP existed. The heated sample was also studied by XRD (Figure 1b) and FT-IR (Supporting Information Figure S6c). Their results demonstrate that the post-treated sample is still pure $LiFePO_4$ phase (JCPDS card no. 81-1173) and PVP has been completely decomposed due to the disappearance of the characteristic absorption peaks of carbonyl. The SEM image, as shown in Figure S7 (Supporting Information), manifests that the dumbbell-like microstructures are completely maintained, indicating the stability of this novel structure.

Figure 7a shows plot of discharge capacity vs cycle number of the calcined $LiFePO_4$ sample at a current rate of C/30. The initial discharge capacity is about 100 mA h g^{-1}, accompanied with a capacity fluctuation between 105 and 115 mA h g^{-1} on the first 40 cycles and then gradually leveling off at 110 mA h g^{-1} after 70 cycles. There is no capacity fading but a slight increase in capacity with increasing cycle number. The results demonstrate the excellent cycling stability of the hierarchically dumbbell-like $LiFePO_4$ microstructures. Figure 7b exhibits charge and discharge curves of the $LiFePO_4$ sample between 4.5 and 2.0 V at a C/30 rate for the first 10 cycles. A flat plateau at 3.4 −3.5 V is observed during both charge and discharge, which corresponds to the two-phase reaction $LiFePO_4 \leftrightarrow (1 - x)LiFePO_4 + xFePO_4 + xLi^+ + xe^-$. The typical charge/discharge voltage profiles of the synthesized $LiFePO_4$ are displayed in Figure 8. In comparison with that of the commercial $LiFePO_4$, the charge and discharge capacities of our sample are much higher than those of the commercial $LiFePO_4$, and the polarization between the charge and discharge plateaus is reduced, indicating that the kinetics of the $LiFePO_4$ are indeed improved partly due to the enhanced electronic conductivity contributed from the carbon layers.[4] Moreover, the comparison for the discharge curves indicates that the plateau for the synthesized $LiFePO_4$ is shorter than the one for the commercial $LiFePO_4$ (40.7% vs 56.3%), whereas the sloping region for the synthesized $LiFePO_4$ is longer correspondingly (59.3% vs 43.7%). As is well-known, the plateau represents a two-phase region (miscibility gap) where two phases, the iron(III) phosphates and lithium iron phosphates, coexist during the Li insertion. Nevertheless, up to now, there has not been a final conclusion about the slope of charge/discharge capacity curves. There are two seemingly credible explanations for the slope. One is considered as a result of the formation of a single-phase solid solution. For example, Meetong et al.[45] carried out comparative electrochemical tests of $LiFePO_4$ nanoparticles of three different sizes: 34, 42, and 113 nm. They found that the solid solution Li_xFePO_4 does not exist for particles with a large

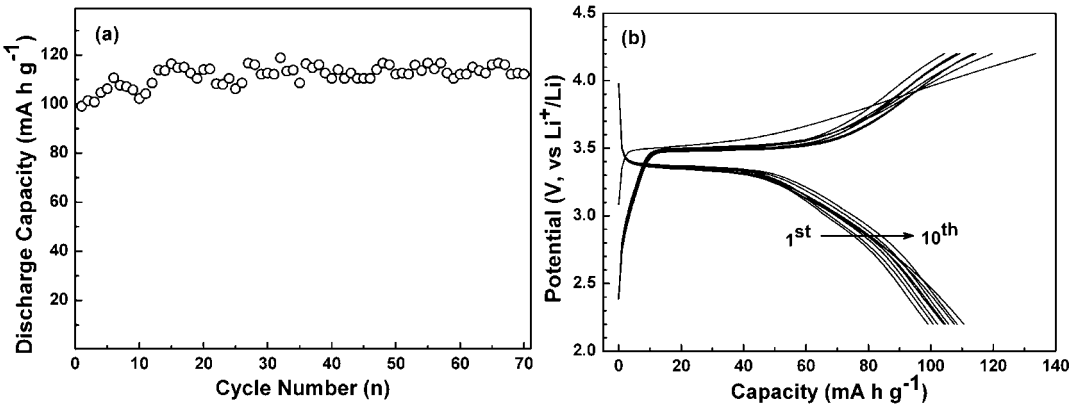

Figure 7. (a) Discharge capacity vs cycle number of $LiFePO_4$ products after calcination at C/30 charge/discharge rates. (b) Charge and discharge profiles of the $LiFePO_4$ sample between 4.5 and 2.0 V at a C/30 rate for the first 10 cycles.

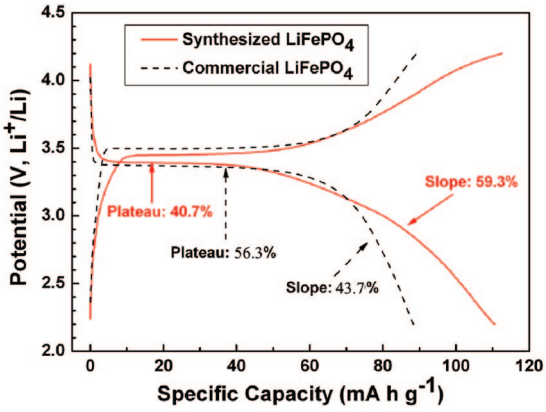

Figure 8. Typical charge/discharge profiles of the synthesized $LiFePO_4$ and the commercial $LiFePO_4$ at a current rate of C/30.

size, and the solid solution can be stabilized only below a critical size which is smaller than 45 nm. Recently, Gibot et al.[46] further confirmed this opinion by the study of the Li insertion/deinsertion process of $LiFePO_4$ nanoparticles with 40 nm. However, in our case, the as-synthesized $LiFePO_4$ microstructures are constructed with nanoplates with ~300 nm length. Therefore, it is not possible to form a solid solution. The other is that the slope is generally considered as capacitive behavior of the surface storage of lithium or interfacial storage of lithium.[47] It is believed that lithium-ion intercalation reactions are the main contributor for the charge/discharge process in the lithium-ion battery. When materials approach nanoscale dimensions, another contribution has to be considered. That is the pseudocapacitive effect, which means the charge storage of lithium ions from faradaic processes occurring at the surface of the materials. In fact, both capacitive behavior and lithium intercalation processes contribute to the total storage of charge with different storage mechanisms.[48] In recent years, the pseudocapacitive effect has been observed in high surface area mesoporous and other nanostructured materials, such as nanostructured TiO_2[49,50] and $LiMn_2O_4$.[51] Our samples are just hierarchically constructed with nanoplates, so it is likely that the particular $LiFePO_4$ structures facilitate the pseudocapacitive behavior. The pronounced capacitive behavior of the synthesized hierarchical microstructures of $LiFePO_4$ may find its use in high-power electrochemical devices as cathode materials. The small capacity of our synthesized $LiFePO_4$ microstructures compared with corresponding theoretical capacity may be attributed to the low electronic conductivity and slow lithium-ion diffusion coefficient, which are the intrinsic character of $LiFePO_4$ materials. And our synthesized material is almost pure phase, and it is not doped with other cations or coated with other electronically conductive materials. In the following work, we will focus on enhancing its electronic conductivity, hence improving its theoretical capacity and rate capability.

4. Conclusion

In this paper, $LiFePO_4$ with hierarchical nanostructures self-assembled by nanoplates is successfully synthesized by using PVP as the surfactant in a benzyl alcohol system. It paves the way for a simple preparation route of $LiFePO_4$, compared with the traditionally multistep methods. The results indicate that both benzyl alcohol and LiI acting as reducing agents promote the formation of $LiFePO_4$ microstructures. The presence of PVP plays an important role in the construction of the hierarchically self-assembled nanostructures. A reasonable formation mechanism is proposed on the basis of the result of time-dependent experiments. In addition, the cell performance of the synthesized $LiFePO_4$ is better than that of the commercial $LiFePO_4$. Its excellent cycling behavior makes it a promising cathode material for advanced electrochemical devices such as lithium-ion batteries and supercapacitor. The methodology will also enlighten a way to prepare other phospholivines such as $LiMnPO_4$ and $LiCoPO_4$.

Acknowledgment. The authors thank the National Natural Science Foundation of China (NSFC, Nos. 20771022, 20701038, 50730005) and the Huo Yingdong Foundation for financial support. This work also was supported by the analysis and testing foundation of Northeast Normal University.

Supporting Information Available: Wide XPS spectrum of $LiFePO_4$ microstructures, typical TEM image of the dumbbell-like $LiFePO_4$ microstructures, detailed XRD patterns of the samples obtained by using water instead of benzyl alcohol as the solvent and replacing LiI by LiCl as Li source with other conditions constant, SEM images of the products prepared with different concentrations of PVP, TEM images of the products obtained with different surfactants, FT-IR spectroscopies of $LiFePO_4$ microstructures, and an SEM image of the $LiFePO_4$ sample obtained after heat treatment at 600 °C. This material is available free of charge via the Internet at http://pubs.acs.org.

References and Notes

(1) Padhi, A. K.; Nanjundaswamy, K. S.; Goodenough, J. B. *J. Electrochem. Soc.* **1997**, *144*, 1188.
(2) Alvaro, C.; Manuel, C. Y.; Julián, M.; Jesús, S. P.; Enrique, R. C. *Eur. J. Inorg. Chem.* **2006**, 1758.

(3) Wang, Y.; Wang, J.; Yang, J.; Nuli, Y. *Adv. Funct. Mater.* **2006**, *16*, 2135.
(4) Hu, Y. S.; Guo, Y. G.; Dominko, R.; Gaberscek, M.; Jamnik, J.; Maiar, J. *Adv. Mater.* **2007**, *19*, 1963.
(5) Franger, S.; Le Cras, F.; Bourbon, C.; Rouault, H. *Electrochem. Solid-State Lett.* **2002**, *5*, A231.
(6) Croce, F.; D'Epifanio, A.; Hassoun, J.; Deptula, A.; Olczac, T.; Scrosati, B. *Electrochem. Solid-State Lett.* **2002**, *5*, A47.
(7) Yang, J.; Xu, J. J. *Electrochem. Solid-State Lett.* **2004**, *7*, A515.
(8) Hsu, K. F.; Tsay, S. Y.; Hwang, B. J. *J. Mater. Chem.* **2004**, *14*, 2690.
(9) Xie, H. M.; Wang, R. S.; Ying, J. R.; Zhang, L. Y.; Jalbout, A. F.; Yu, H. Y.; Yang, G. L.; Pan, X. M.; Su, Z. M. *Adv. Mater,* **2006**, *18*, 2609.
(10) Wang, L.; Li, Z.; Xu, H.; Zhang, K. *J. Phys. Chem. C* **2008**, *112*, 308.
(11) Islam, M. S.; Driscoll, D. J.; Fisher, C. A. J.; Slater, P. R. *Chem. Mater.* **2005**, *17*, 5085.
(12) Ravet, N.; Gauthier, M.; Zaghib, K.; Goodenough, J. B.; Mauger, A.; Gendron, F.; Julien, C. M. *Chem. Mater.* **2007**, *19*, 2595.
(13) Allen, J. L.; Jow, T. R.; Wolfenstine, J. *Chem. Mater.* **2007**, *19*, 2108.
(14) Gaberscek, M.; Küzma, M.; Jamnik, J. *Phys. Chem. Chem. Phys.* **2007**, *9*, 1815.
(15) Kang, H. C.; Jun, D. K.; Jin, B.; Jin, E. M.; Park, K. H.; Gu, H. B.; Kim, K. W. *J. Power Sources* **2008**, *179*, 340.
(16) Ellis, B.; Kan, W. H.; Makahnouk, W. R. M.; Nazar, L. F. *J. Mater. Chem.* **2007**, *17*, 3248.
(17) Dokko, K.; Koizumi, S.; Kanamura, K. *Chem. Lett.* **2006**, *35*, 338.
(18) Dokko, K.; Koizumi, S.; Nakano, H.; Kanamura, K. *J. Mater. Chem.* **2007**, *17*, 4803.
(19) Rhodes, K. H.; Davis, S. A.; Caruso, F.; Zhang, B.; Mann, S. *Chem. Mater.* **2000**, *12*, 2832.
(20) Kim, F.; Kwan, S.; Akana, J.; Yang, P. *J. Am. Chem. Soc.* **2001**, *123*, 4360.
(21) Fan, X.; Meng, X. M.; Zhang, X. H.; Shi, W. S.; Zhang, W. J.; Zapien, J. A.; Lee, C. S.; Lee, S. T. *Angew. Chem., Int. Ed.* **2006**, *45*, 2568.
(22) Wu, J.; Duan, F.; Zheng, Y.; Xie, Y. *J. Phys. Chem. C* **2007**, *111*, 12866.
(23) Zhang, X.; Ai, Z.; Jia, F.; Zhang, L. *J. Phys. Chem. C* **2008**, *112*, 747.
(24) Prosini, P. P.; Carewska, M.; Scaccia, S.; Wisniewski, P.; Passerini, S.; Pasquali, M. *J. Electrochem. Soc.* **2002**, *149*, A886.
(25) Huang, H.; Yin, S. C.; Nazar, L. F. *Electrochem. Solid-State Lett.* **2001**, *4*, A170.
(26) Dominko, R.; Bele, M.; Goupil, J. M.; Gaberscek, M.; Hanzel, D.; Arcon, I.; Jamnik, J. *Chem. Mater.* **2007**, *19*, 2960.
(27) Jia, F.; Zhang, L.; Shang, X.; Yang, Y. *Adv. Mater.* **2008**, *20*, 1050.
(28) Pinna, N.; Grancharov, S.; Beato, P.; Bonville, P.; Antonietti, M.; Niederberger, M. *Chem. Mater.* **2005**, *17*, 3044.
(29) Pinna, N.; Neri, G.; Antonietti, M.; Niederberger, M. *Angew. Chem., Int. Ed.* **2004**, *43*, 4345.
(30) Niederberger, M. *Acc. Chem. Res.* **2007**, *40*, 793.
(31) Niederberger, M.; Pinna, N.; Polleux, J.; Antonietti, M. *Angew. Chem., Int. Ed.* **2004**, *43*, 2273.
(32) Shiraishi, K.; Dokko, K.; Kanamura, K. *J. Power Sources* **2005**, *146*, 555.
(33) Bhuvaneswari, M. S.; Bramnik, N. N.; Ensling, D.; Ehrenberg, H.; Jaegermann, W. *J. Power Sources* **2008**, *180*, 553.
(34) Burba, C. M.; Frech, R. *J. Electrochem. Soc.* **2004**, *151*, A1032.
(35) Salah, A. A.; Jozwiak, P.; Zaghib, K.; Garbarczyk, J.; Gendron, F.; Mauger, A.; Julien, C. M. *Spectrochim. Acta, Part A* **2006**, *65*, 1007.
(36) Wang, J. W.; Wang, X.; Peng, Q.; Li, Y. D. *Inorg. Chem.* **2004**, *43*, 7552.
(37) Nemamcha, A.; Rehspringer, J. L.; Khatmi, D. *J. Phys. Chem. B* **2006**, *110*, 383.
(38) Li, Y.; Liu, J.; Huang, X.; Li, G. *Cryst. Growth Des.* **2007**, *7*, 1350.
(39) Suber, L.; Sondi, I.; Matijević, E.; Goia, D. V. *J. Colloid Interface Sci.* **2005**, *288*, 489.
(40) Xu, T. G.; Zhang, C.; Shao, X.; Wu, K.; Zhu, Y. F. *Adv. Funct. Mater.* **2006**, *16*, 1599.
(41) Zeng, J.; Xin, M. D.; Li, K. W.; Wang, H.; Yan, H.; Zhang, W. J. *J. Phys. Chem. C* **2008**, *112*, 4159.
(42) Hu, X.; Yu, J. C. *Adv. Funct. Mater.* **2008**, *18*, 880.
(43) Chen, H. L.; Grey, C. P. *Adv. Mater.* **2008**, *20*, 2206.
(44) Zhuang, J. L.; Liang, L. F.; Sung, H. H. Y.; Yang, X. F.; Wu, M. M.; Williams, I. D.; Feng, S. H.; Su, Q. *Inorg. Chem.* **2007**, *46*, 5404.
(45) Meetong, N.; Huang, H.; Carter, W. C.; Chiang, Y. M. *Electrochem. Solid-State Lett.* **2007**, *10*, A134.
(46) Gibot, P.; Cabanas, M. C.; Laffont, L.; Levasseur, S.; Carlach, P.; Hamelet, S.; Tarascon, J. M.; Masquelier, C. *Nat. Mater.* **2008**, *7*, 741.
(47) Maier, J. *Nat. Mater.* **2005**, *4*, 805.
(48) Winter, M.; Brodd, R. J. *Chem. Rev.* **2004**, *104*, 4245.
(49) Wang, J.; Polleux, J.; Lim, J.; Dunn, B. *J. Phys. Chem. C* **2007**, *111*, 14925.
(50) Zhang, H.; Li, G. R.; An, L. P.; Yan, T. Y.; Gao, X. P.; Zhu, H. Y. *J. Phys. Chem. C* **2007**, *111*, 6143.
(51) Luo, J. Y.; Wang, Y. G.; Xiong, H. M.; Xia, Y. Y. *Chem. Mater.* **2007**, *19*, 4791.

JP808080T

Supporting Information for:

Solvothermal synthesis of $LiFePO_4$ hierarchically dumbbell-like microstructures by nanoplate self-assembly and their application as a cathode material in lithium-ion batteries

Hui Yang[†], Xing-Long Wu[ζ,,§], Min-Hua Cao[†,‡*], Yu-Guo Guo[ζ,*]

[†]Department of Chemistry, Northeast Normal University, Changchun, 130024, P. R. China, E-mail: caomh043@nenu.edu.cn

[‡]Department of Chemistry, Beijing Institute of Technololy, Beijing, 100081, P. R. China.

[ζ]Beijing National Laboratory for Molecular Sciences, Institute of Chemistry, Chinese Academy of Sciences, Beijing 100190, China, E-mail: ygguo@iccas.ac.cn

[§] Also at the Graduate School of CAS, Beijing 100064, China

Figure S1 Wide XPS spectrum of $LiFePO_4$ microstructures.

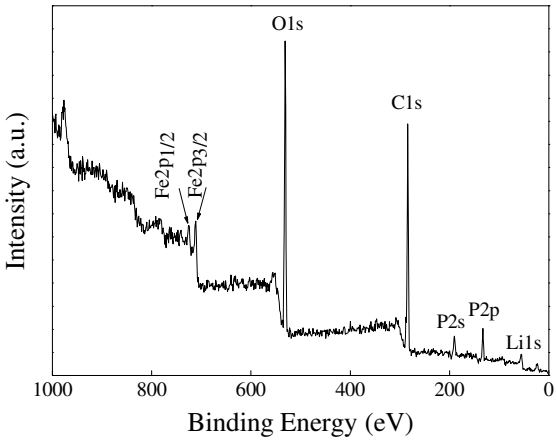

Figure S2 Typical TEM image of the dumbbell-like $LiFePO_4$ microstructures

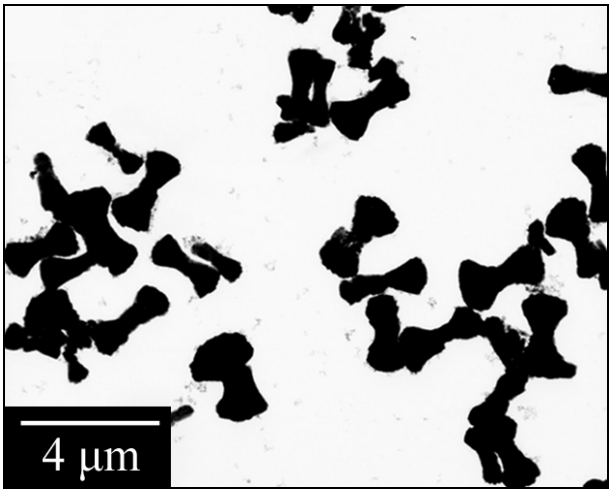

Figure S3 Detailed XRD patterns of the samples obtained by (a) using water instead of benzyl alcohol as the solvent (b) replacing LiI by LiCl as Li source with other conditions constant.

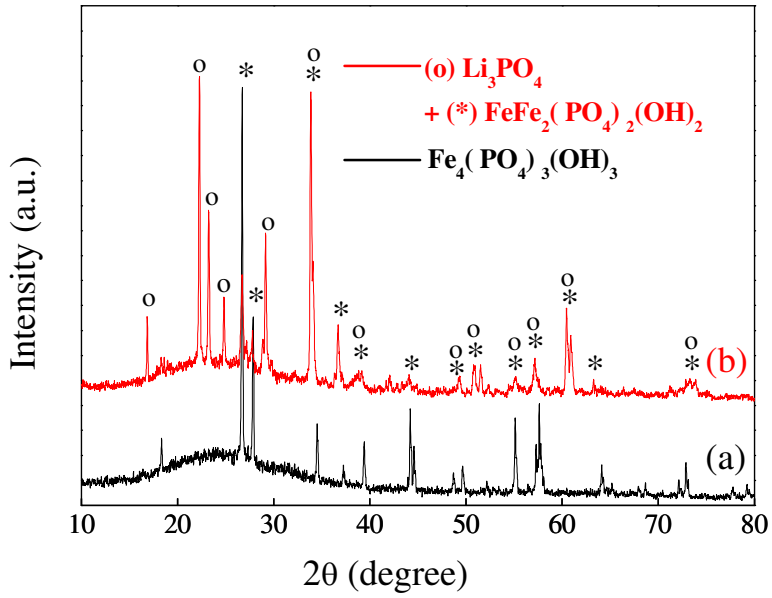

Figure S4 SEM images of the products prepared with different concentrations of PVP (a) no PVP, (b) 0.021 M (c) 0.029 M (d) 0.037 M.

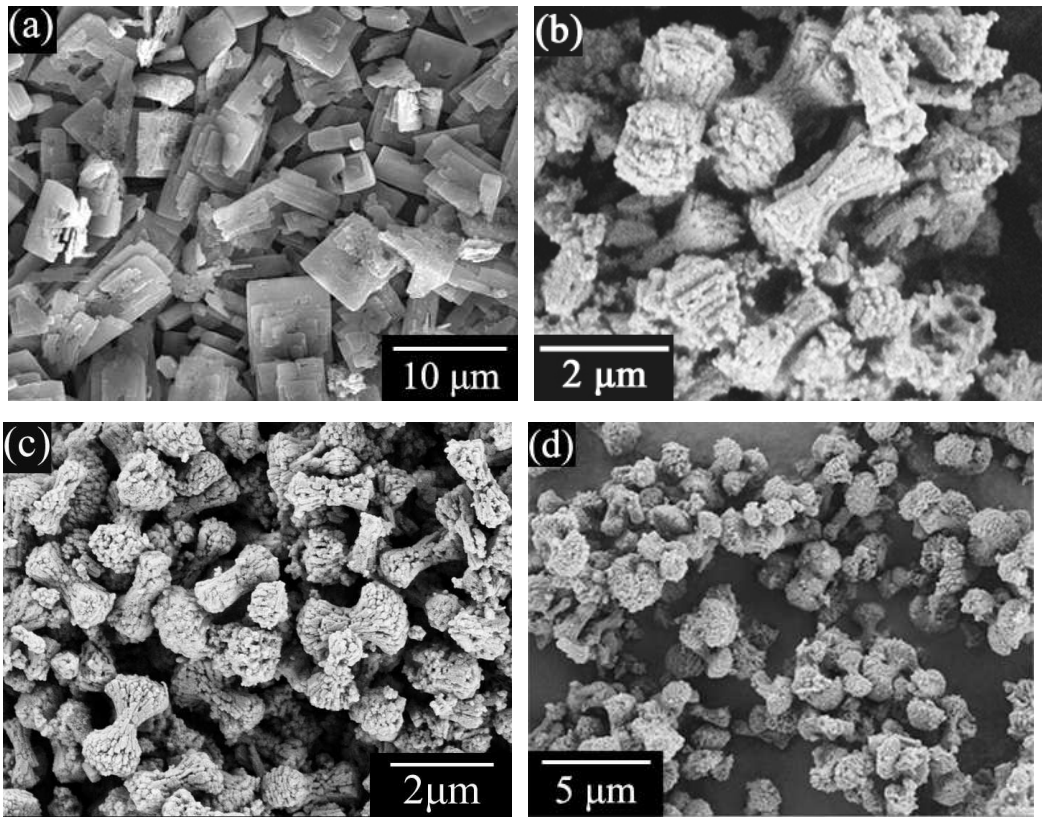

Figure S5 The TEM images of the products obtained with different surfactants (a) CTAB (b) PEG (c) TX-100

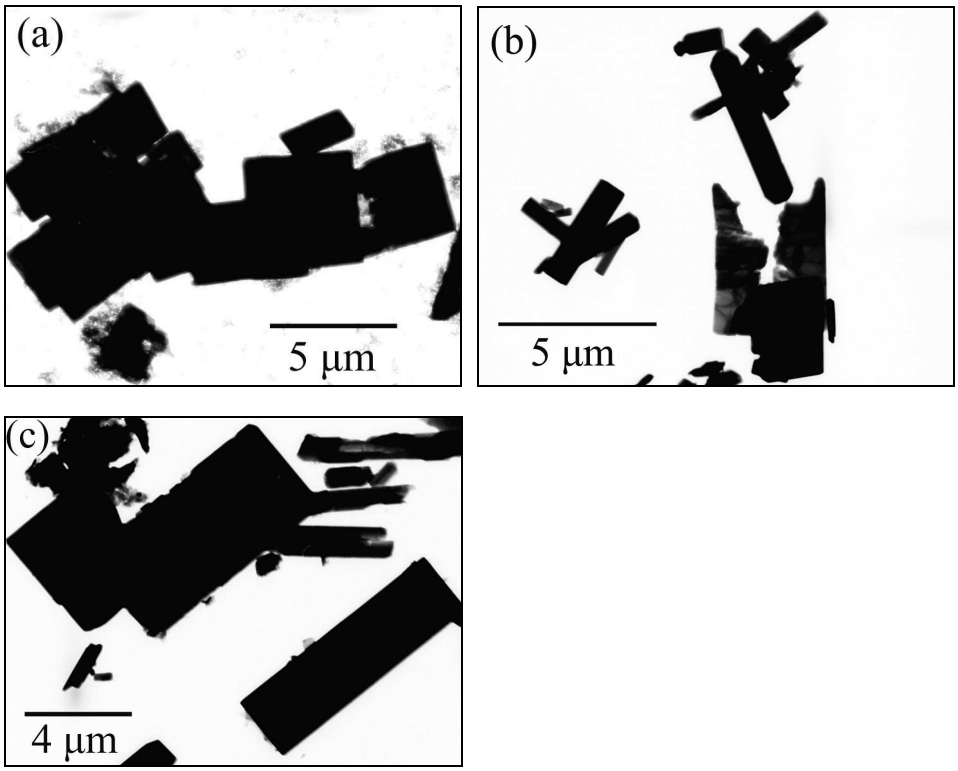

Figure S6 FT-IR spectroscopies of (a) hierarchically dumbbell–like $LiFePO_4$ microstructures, (b) pure PVP and (c) $LiFePO_4$ sample obtained after heat treatment at 600 °C.

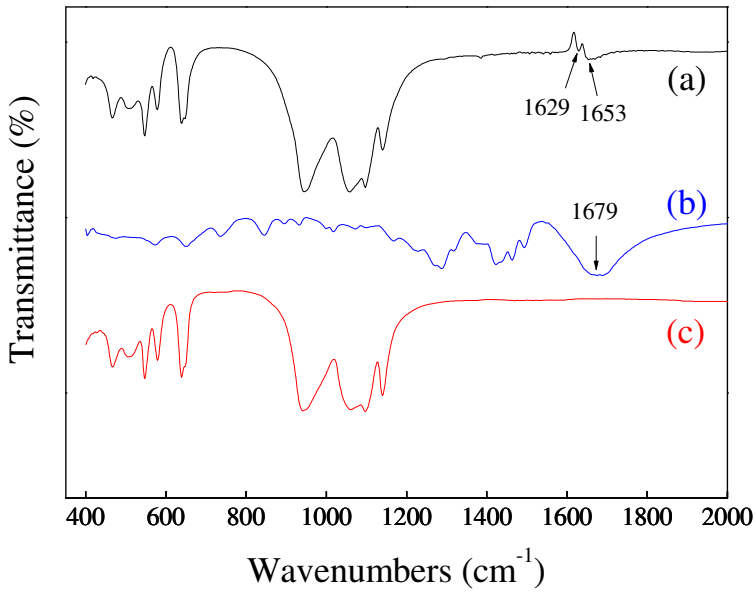

Figure S7 SEM image of $LiFePO_4$ sample obtained after heat treatment at 600 °C.